Geomechanics and Engineering, *Vol. 14, No. 2 (2018) 141-149*
DOI: https://doi.org/10.12989/gae.2018.14.2.141

Analysis on the creep response of bolted rock using bolted burgers model

Tong-Bin Zhao[1a], Yu-Bao Zhang[1b], Qian-Qing Zhang[*2] and Yun-Liang Tan[1c]

[1]*State Key Laboratory of Mining Disaster Prevention and Control Co-founded by Shandong Province and the Ministry of Science and Technology, Shandong University of Science and Technology, Qingdao, Shandong 266590, PR China*
[2]*Geotechnical and Structural Engineering Research Center, Shandong University, Jinan, Shandong 250061, PR China*

(Received May 15, 2016, Revised May 30, 2017, Accepted July 3, 2017)

Abstract. In this paper, the creep behavior of bolted rock was analyzed by using the unconfined creep tests and the numerical results. Based on the test results, the Bolted Burgers creep model (B-B model) was proposed to clarify the creep mechanism of rock mass due to rock bolts. As to the simulation of the creep behaviour of bolted rock, a new user-defined incremental iterative format of the B-B model was established and the open-source FLAC^{3D} code was written by using the object-oriented language (C++). To check the reliability of the present B-B creep constitutive model program, a numerical model of a tunnel with buried depth of 1000 m was established to analyze the creep response of the tunnel with the B-B model support, the non-support and the bolt element support. The simulation results show that the present B-B model is consistent with the calculated results of the inherent bolt element in FLAC^{3D}, and the convergence deformation can be more effectively controlled when the proposed B-B model is used in the FLAC^{3D} software. The big advantage of the present B-B creep model secondarily developed in the FLAC^{3D} software is the high computational efficiency.

Keywords: bolted rock; creep test; Bolted Burgers model; FLAC^{3D} secondary development

1. Introduction

The stability of surrounding rock of tunnel has been a subject of intensive study in underground engineering for many years (Tan *et al*. 2015, 2017, Zhao *et al*. 2016, 2017), because the failure of tunnel is of great concern in evaluating the safety of engineering structures and geological engineering facilities. The rock bolts as an effective supporting technique have now been widely utilized for the stability of surrounding rock of tunnel in China. The currently available techniques for the analysis of rock bolts largely concentrate on the estimation of the interactive behavior of bolt and rock mass. Spang and Egger (1990) explained the mode of action of fully-bonded, untensioned rock bolts in stratified or jointed rock masses. Chen *et al*. (2004) formulated a three dimensional elasto-viscoplastic composite element method for rock masses reinforced by a fully-grouted bolt. Cai *et al*. (2004) developed an analytical model for rock bolts based on an improved Shear-Lag Model and proposed a method to analyze the interaction behavior of the rock bolt and the surrounding rock mass. Deb and Das (2014) developed a doubly enriched finite element procedure by introducing strong displacement discontinuities in the form of rock joints and reinforcement affect in the form of rock bolts. Nemcik *et al*. (2014) presented a numerical model of fully grouted rock bolts loaded in tension by implementing a non-linear bond-slip relationship of bolt-grout interface into a commercial finite difference rock mechanics code. Showkati *et al*. (2015) presented a new theoretical method for analysis of stress around a tensioned anchor in rock which considers both the anchor head bearing plate and its grouted bond length embedded in depth. Progress has also been made in the investigation of the supporting design of rock bolts in underground engineering (Cai *et al*. 2015, Zhang *et al*. 2015, Boon *et al*. 2015, Kang *et al*. 2015).

However, little consideration has been given to the examination of time-dependent effects in the bolted rock mass. The creep problems such as supporting system failure and cavern large deformation caused by high ground stress are common in practice and difficult to control (Sun 2007, Wang *et al*. 2015, Lopez-Gayarre *et al*. 2015). Although the time-dependent response of deep rigid anchor (Selvadurai 1978), prestress in a surface rock anchor (Selvadurai 1979), and epoxy-bonded anchor system (Yang *et al*. 2014) were studied, the creep behavior of bolted rock is seldom mentioned and characterized in the literature. To decrease the creep deformation of deep-lying rock mass, and guarantee the security of underground engineering, there is a need to clarify the effect on creep behavior of rock on account of rock bolts.

In this paper, the unconfined creep tests were carried out to analyze the creep behavior of the non-bolted red sandstones and the bolted red sandstones, and propose the failure modes of bolted rock. The Bolted Burgers creep constitutive model was then proposed to describe the creep

∗Corresponding author, Ph.D.
E-mail: zjuzqq@163.com
[a]Associate Professor
E-mail: ztbwh2001@163.com
[b]Ph.D. Student
E-mail: zybsdust@163.com
[c]Professor
E-mail: tylllp@163169.net

ISSN: 2005-307X (Print), 2092-6219 (Online)

behavior of bolted rock. As to the numerical simulation, the B-B creep model was subsequently developed in the FLAC^{3D} software by using a VC++ code. To check the reliability of the proposed B-B constitutive model, a numerical model of a deep-lying tunnel was established to analyze the creep behavior of the tunnel.

2. Creep experiments

2.1 Specimen preparation

The test specimens of red sandstone were cored from Jining mine buried at -1000 m level, Shandong Province, China. The red sandstones were cut into standard rock specimens with 50 mm diameter and 100 mm height, and used as the basal body of bolted rock structure. The mechanical properties of red sandstones are presented in Table 1. Note that the selection of bolt and bonding material is important in the creep test of bolted rock structures. In practice, the bolt can be simulated by using the iron wire, copper wire, lead wire or mao bamboo, and the cement mortar, chemical grout or artificial ingredients can be used as bonding material in laboratory tests (Wen 2007, Chen 2008). Due to high tensile strength, variable stiffness and easy processability of the mao bamboo, the mao bamboo can be commonly used as the bolt, as shown in Fig. 1. Based on the test results (see Table 2) (Wen 2007), the mao bamboo was selected to simulate the bolt in the present study, and the binder was made of blanc fixe, rosin and alcohol with the weight ratio of 10:1:2. It should be pointed out that the behavior of bolted material can not completely satisfy the similarity theory for practical purposes, however, comparing Table 1 with Table 2, it can be concluded that the mao bamboo can be used to simulate the bolt in bolted red sandstone.

2.2 Installing parameters of bolt

In practice, the diameter of the bolt commonly used was 20 mm, the drilling diameter of the bolt was adopted as 32 mm, and the spacing between two bolts was 800 mm. In this paper, the bolt commonly used in practice was used as prototype. Based on the geometric similarity ratio of 8:1, in the model test the drilling diameter of the mao bamboo bolt was adopted as 4 mm, the dimension of the mao bamboo bolt used in the model test was adopted as 2.5 mm in diameter, and 100 mm in the mao bamboo bolt spacing, as shown in Table 3. The mao bamboo surface is carved with symmetrical two rows of burrs to enhance the bond between the bamboo bolt and the bonding material. The bolted red sandstone specimens are shown in Fig. 2.

2.3 Testing procedure

The unconfined creep tests were carried out by using a servo-hydraulic RLJW-2000 rheological test system (see Fig. 3). For the multistage unconfined creep tests, the load was used as the feedback signal. The load ratio was adopted as 50 N/s. In multistage tests, the load was recorded after the load had been applied and maintained for 24 h at each load step. At each load step, the specimens were under sustained load conditions, and the load was recorded every 1min. The axial strain and horizontal strain can be acquired continuously by extensometers and digital dial gauges, respectively.

The magnitude of load at the first step was selected as 1/5 of the uniaxial compressive strength, σ_c. At the subsequent load steps, the load was increased by 0.05 to 0.1 times σ_c. The loading scheme is listed in Table 4. After n load steps, the creep damage of specimen was assumed to occur. In the tests, the room temperature was maintained at 25℃.

Table 1 Mechanical properties of the red sandstone

Specimens	Elastic modulus (GPa)	Poisson's ratio	Compressive strength (MPa)
1-1-1	5.32	0.24	42.84
1-1-2	4.98	0.22	46.96
1-1-3	5.08	0.27	50.15
1-1-4	4.86	0.24	48.95
1-1-5	4.50	0.23	45.10
Average	4.95	0.24	46.80

Table 2 Mechanical properties of the mao bamboo

Specimens	Elastic modulus (GPa)	Tensile Strength (MPa)
01	9.48	120.67
02	10.40	128.67
03	10.42	147.47
Average	10.10	132.05

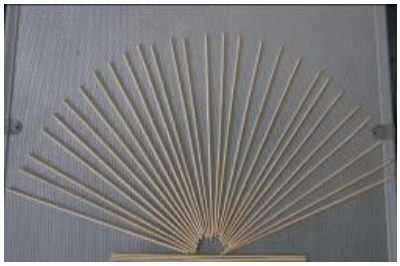

Fig. 1 Mao bamboo bolt

Table 3 Installing parameters of bolt in specimen

Category	Drilling diameter (mm)	Bolt diameter (mm)	Spacing (mm)
Non-bolted specimen	32	20	800×800
Bolted specimen	4	2.5	100×100

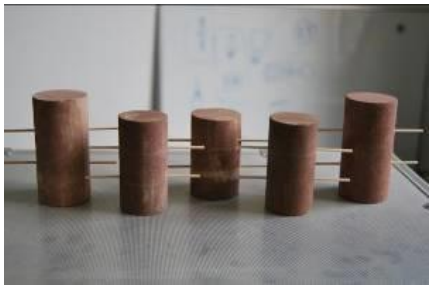

Fig. 2 Bolted red sandstone specimens

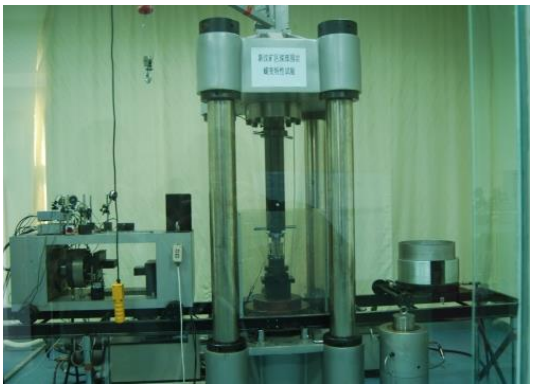

Fig. 3 RLJW-2000 rheological test system

Table 4 Loading scheme of the creep test

No.	Stress level	Range	Load interval	Comment
1	Low stress	0-40% σ_c	10% σ_c	When axial creep deformation exceed 0.001 mm/h at high stress level, the load interval is 5% σ_c, otherwise the load interval is 10% σ_c
2	Medium stress	40-70% σ_c	10% σ_c	
3	High stress	70-100% σ_c	5~10% σ_c	

Table 5 Creep test results of two kinds of red sandstones

Category	Number	Step load times	Stress threshold of initial creep (%)	Stress level of creep failure (%)	Test time (h)	Failure way
Non-bolted specimens	1-1	7	20% σ_c	80% σ_c	167.0	Skew split
	1-2	8	20% σ_c	85% σ_c	175.3	Blast split
Bolted specimens	2-1	8	50% σ_c	90% σ_c	174.5	Weak shear
	2-2	8	40% σ_c	90% σ_c	174.9	Weak shear

2.4 Experimental results and discussion

Two non-bolted red sandstone specimens and two bolted red sandstone specimens were carried out by using the uniaxial compression creep tests, lasting 691.7 h. The experimental results are shown in Table 5. Fig. 4 shows the relationship between axial and horizontal creep strains and time for each stage of the specimens. From Fig. 4 it can be seen that the mechanical property of red sandstones can be great improved, and the deformation of bolted specimens is smaller than the non-bolted specimens under the same loading level. This suggests that the axial and horizontal creep strains of specimens can be obviously restrained by bolts. Under a medium stress level, the creep of bolted specimen can be observed. However, the creep of non-bolted specimen can be investigated at low stress level. It can be concluded that the creep stress level of bolted specimen is 1.2 to 1.3 times that of the non-bolted specimens and the threshold of creep stress is large because of the anchoring effect of bolts. At high stress level, a large creep rate of the bolted specimen is observed when the load is 0.9 times σ_c. Compared with the bolted specimen, the creep deformation of the non-bolted specimen increases significantly when the load increase from 70% σ_c to 80% σ_c.

As shown in Fig. 5, the failure modes of non-bolted specimen and bolted specimen are split and shear, respectively. It is noteworthy that the rock failure mode is transformed from vertical splitting to weak shear by reason of the presence of the bolts. For the non-bolted specimens,

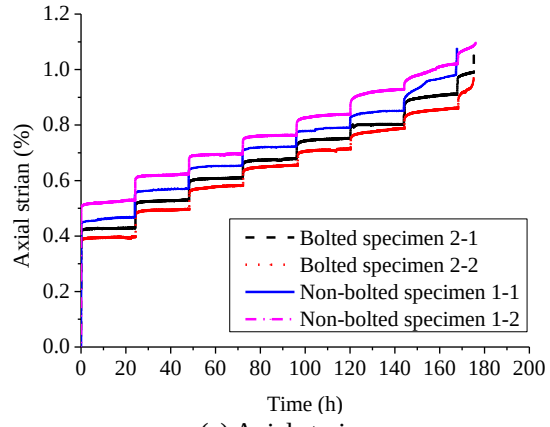

(a) Axial strain

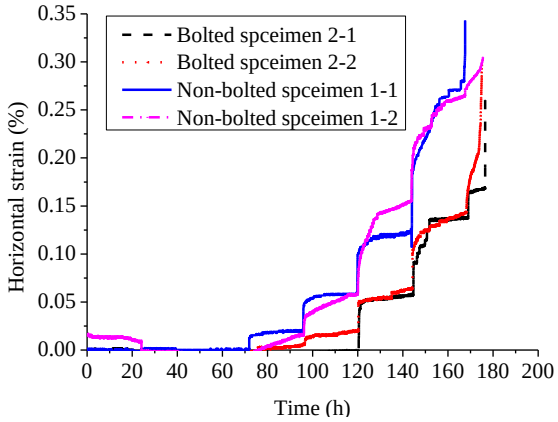

(b) Horizontal strain

Fig. 4 Creep strains of two kinds of red sandstone under load

(a) Non-bolted specimen

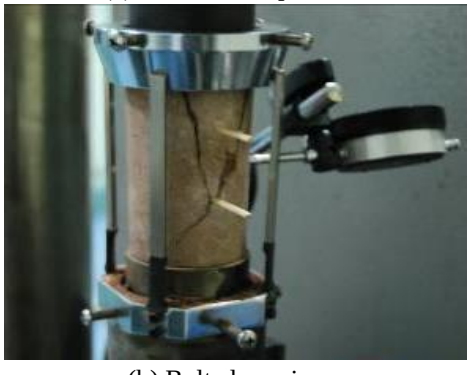

(b) Bolted specimen

Fig. 5 Failure modes of rock specimens in creep test

the creep failure occurred when the load was 0.8 to 0.85 times σ_c, while the creep failure of the bolted specimens occurred when the load was 0.9 times σ_c. This suggests that the strength of red sandstones can be improved due to the anchoring effect of bolts, and the failure strength of the bolted specimen is 1.05 to 1.1 times that of the non-bolted specimen.

3. Creep mechanism of bolted rock

There are various combination forms between the way of bolting and the direction of load as shown in Fig. 6. To consider the integrality of bolted rock and simplify the calculation, the bolt is assumed to be equivalent to a multiple spring with great stiffness. It can be concluded that the creep characteristics of the bolted red sandstone can be simulated using the Burgers model (see Fig. 4). The B-B creep constitutive model is proposed to describe the bolted rock as shown in Fig. 7.

Based on the interaction between of bolts and rock, the deformation of bolts is assumed to be identical to that of rock and the load is shared by bolts and rock. One obtains

$$\begin{cases} \varepsilon_{br} = \varepsilon_r = \varepsilon_b \\ \sigma_{br} = \sigma_r + \sigma_b \end{cases} \tag{1}$$

where ε_{br} is the strain of bolted rock, ε_r is the strain of rock, ε_b is the strain of bolt, σ_{br} is the stress of bolted rock, σ_r is the stress of rock, and σ_b is the stress of bolt.

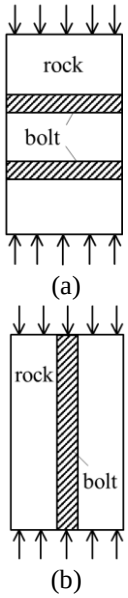

Fig. 6 Common distribution of bolts

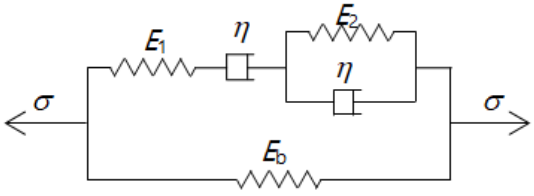

Fig. 7 Present B-B creep constitutive model

The constitutive relationship of the Burgers model can be written as

$$\sigma_r + p_1\dot{\sigma}_r + p_2\ddot{\sigma}_r = q_1\dot{\varepsilon}_r + q_2\ddot{\varepsilon}_r \tag{2}$$

where $p_1=\eta_1/E_1+(\eta_1+\eta_2)/E_2$, $p_2=\eta_1\eta_2/E_1E_2$, $q_1=\eta_1$, and $q_2=\eta_1\eta_2/E_2$. $\dot{\sigma}_r$ is the derivative of σ_r, $\ddot{\sigma}_r$ is the second derivative of σ_r, $\dot{\varepsilon}_r$ is the derivative of ε_r, $\ddot{\varepsilon}_r$ is the second derivative of ε_r. E_1 and E_2 are the stiffness of the two springs in the Burgers model. η_1 and η_2 are the viscosity of the two dashpots in the Burgers model.

The constitutive relationship of the bolt can be expressed as

$$\sigma_b = E_b\varepsilon_b \tag{3}$$

where E_b is the the stiffness of the bolt.

By inserting Eqs. (2)-(3) into Eq. (1), the following equation can be obtained

$$\sigma_{br} + p_1\dot{\sigma}_{br} + p_2\ddot{\sigma}_{br} = E_b\varepsilon_{br} + (q_1 + p_1E_b)\dot{\varepsilon}_{br} + (q_2 + p_2E_b)\ddot{\varepsilon}_{br} \tag{4}$$

where $\dot{\sigma}_{br}$is the derivative of σ_{br}, $\ddot{\sigma}_{br}$is the second derivative of σ_{br}, $\dot{\varepsilon}_{br}$is the derivative of ε_{br}, $\ddot{\varepsilon}_r$ is the second derivative of ε_{br}.

When the value of σ_{br} is equal to the value of σ_0, and the values of σ_{br} and σ_0 are a constant value, Eq. (4) can be rewritten as

$$\alpha\ddot{\varepsilon}_{br} + \beta\dot{\varepsilon}_{br} + \lambda\varepsilon_{br} - \sigma_0 = 0 \tag{5}$$

where $\alpha = q_2 + p_2E_b$, $\beta = q_1 + p_1E_b$, and $\lambda = E_b$.

The one-dimensional constitutive relationship of B-B model can be proposed from the following form

$$\varepsilon_{br} = Ae^{r_1t} + Be^{r_2t} + C \tag{6}$$

where $r_1 = \frac{-\beta + \sqrt{\beta^2 - 4\alpha\lambda}}{2\alpha}$, $r_2 = \frac{-\beta - \sqrt{\beta^2 - 4\alpha\lambda}}{2\alpha}$, and $C = \frac{\sigma_0}{\lambda}$.

The initial conditions of the B-B model can be expressed as the following forms

$$t=0,\ \varepsilon_{br} = \frac{\sigma_0}{E_1 + E_b} \tag{7}$$

$$t=0,\ \dot{\varepsilon}_{br} = \sigma_0\left(\frac{1}{\eta_1} + \frac{1}{\eta_2}\right)\frac{E_1}{E_1 + E_b} \tag{8}$$

Based on Eqs. (6)-(8), the values of A, B and D can be calculated as

$$A = \frac{1}{r_1 - r_2}\left(D - r_2\left(\frac{\sigma_0}{E_1 + E_b} - C\right)\right) \tag{9}$$

$$B = \frac{1}{r_2 - r_1}\left(D - r_1\left(\frac{\sigma_0}{E_1 + E_b} - C\right)\right) \tag{10}$$

$$D = \sigma_0\left(\frac{1}{\eta_1} + \frac{1}{\eta_2}\right)\frac{E_1}{E_1 + E_2} \tag{11}$$

Based on the compatible deformation of bolt and rock, the influence of support effect of bolt on the creep of rock can be summarized as two aspects: (i) The load supported

by the surrounding rock will decrease due to more loads shared by the bolts, and the creep behavior of rock will be weakened; and (ii) the constrained effects of deformation and creep rate of the bolted rock are significantly enhanced and the overall deformation of rock decreases, because the interaction of bolts and rock increases with increasing stiffness of bolts.

The experimental results of the non-bolted rock specimen 1-1 and the bolted rock specimen 2-1 at the stress level of 0.7 times σ_c are analyzed to clarify the creep behavior of the bolted rock. The back-analyzed creep parameters of the Burgers model are summarized as below: E_1 = 101.619 MPa, η_1=313524.256 MPa·min, E_2=2556.645 MPa, and η_2=27771.188 MPa·min. Based on the ratio of the bolt area to the rock area, and the parameters listed in Table 2 and Table 3, the equivalent stiffness of the mao bamboo bolt E_b can be adopted as 32.167 MPa. The calculated and the experimental creep strains are shown in Fig. 8. Fig. 8 demonstrates that the creep properties of bolted surrounding rock can be well simulated by using the B-B model.

In the analysis of the influence of the equivalent stiffness of bolts on the creep strain, the equivalent stiffness of the bolts, E_b', is defined as ξ times E_b. The value of ξ is defined as the density of bolting. When the value of ξ is adopted as 1, 2, 3, 4, 5, the creep strains of surrounding rock are shown in Fig. 9.

Fig. 9 shows that the creep strain of bolted rock decreases with increasing density of bolting, ξ. When the value of ξ is adopted as 2, the incremental deformation and total deformation of bolted rock substantially decrease.

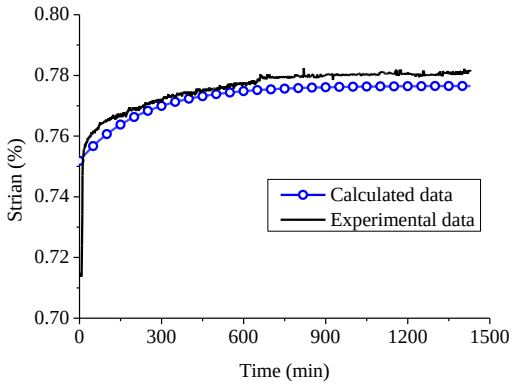

Fig. 8 Calculated and experimental creep strains

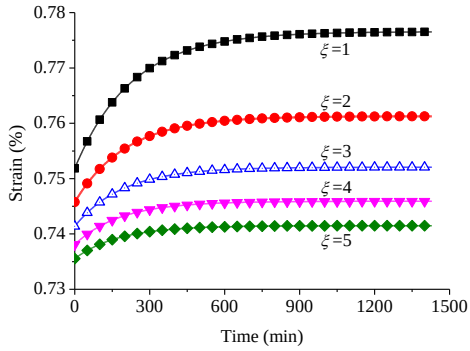

Fig. 9 Creep strain with different values of ξ for the B-B model

When the value of ξ is adopted as 4 or 5, the incremental deformation is small and the creep characteristics of the bolted rock are not obvious.

4. Analysis on the numerical results

4.1 Secondary development in FLAC3D by using B-B model

To build a new user-defined constitutive model adopted in FLAC^{3D}, the relationship of finite difference between stress increment and strain increment with time should be established. According to the elastic-plastic theory, the spherical tensor of stress is in hydraulic stress state, and only varies due to the variation of volume of object. The deviatoric stress tensor only changes with the variation of shape of object. The creep behavior of rock is supposed to be caused only by the deviatoric stress tensor.

For the Maxwell model, the increment of deviatoric strain tensor, Δe_{ij}^{M}, can be described as

$$\Delta e_{ij}^{M}=\frac{S_{ij}^{M,N}-S_{ij}^{M,O}}{2G_1}+\frac{(S_{ij}^{M,N}+S_{ij}^{M,O})\Delta t}{4\eta_1} \tag{12}$$

where $S_{ij}^{M,N}$ is the new deviatoric stress tensor of the Maxwell model for a time step, $S_{ij}^{M,O}$ is the old deviatoric stress tensor of the Maxwell model for a time step, and G_1 is the three dimensional elastic parameter of the Maxwell model.

The Kelvin model, also called Voigt model, is widely used in geotechnical engineering (Wu *et al*. 2014). For the Kelvin model, the increment of deviatoric strain tensor, Δe_{ij}^{K}, can be described as

$$\Delta e_{ij}^{K}=\frac{1}{A}\left[\left(S_{ij}^{K,N}+S_{ij}^{K,O}\right)\Delta t-(A+B)e_{ij}^{K,O}\right] \tag{13}$$

where A=2$G_2\Delta t$+4η_2, B=2$G_2\Delta t$−4η_2, $S_{ij}^{K,N}$ is the new deviatoric stress tensor of the Kelvin model for a time step, $S_{ij}^{K,O}$ is the old deviatoric stress tensor of the Kelvin model for a time step, $e_{ij}^{K,O}$ is the old deviatoric strain tensor of the Kelvin model for a time step, and G_2 is the three dimensional visco-elastic parameter of the Kelvin model.

The Burgers model can be assumed to be composed of the Kelvin model and the Maxwell model. The deviatoric stress tensor and the increment of deviatoric strain tensor of the Burgers model can be described as

$$S_{ij}=S_{ij}^{M}=S_{ij}^{K} \tag{14}$$

$$\Delta e_{ij}=\Delta e_{ij}^{M}+\Delta e_{ij}^{K} \tag{15}$$

The new deviatoric stress tensor of the Burgers model can be derived from Eqs.(12)-(15) and expressed as

$$S_{ij}^{N}=\frac{1}{X}\left[\Delta e_{ij}+YS_{ij}^{O}-\left(\frac{B'}{A'}-1\right)e_{ij}^{K,O}\right] \tag{16}$$

where $X=\frac{\Delta t}{4A'\eta_2}+\frac{1}{2G_1}+\frac{\Delta t}{4\eta_1}$, $A'=1+\frac{G_2\Delta t}{2\eta_2}$, $Y=\frac{1}{2G_1}-\frac{\Delta t}{4\eta_1}-\frac{\Delta t}{4A'\eta_2}$, and $B'=1-\frac{G_2\Delta t}{2\eta_2}$.

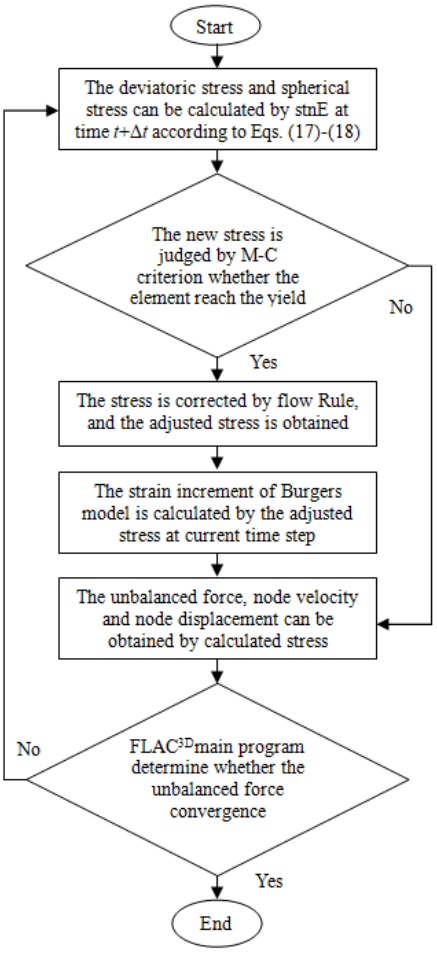

Fig. 10 Program flowchart of the B-B creep model

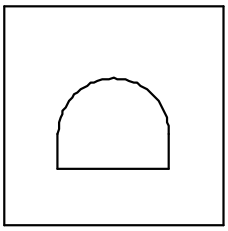

(a) Non-support

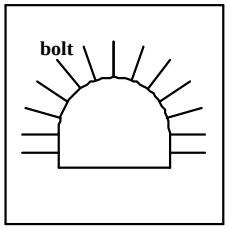

(b) Bolt element

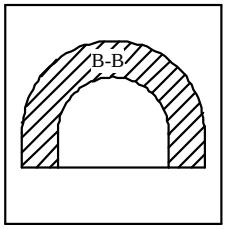

(c) B-B model

Fig. 11 Schematic diagram of calculation model

The B-B model is composed of the Burgers model in parallel with a bolt model (see Fig. 7). The new deviatoric stress tensor of B-B model is proposed

$$S_{ij}^{N}=\frac{1}{X}\left[(1+2G_{\mathrm{b}}X)\Delta e_{ij}+YS_{ij}^{O}+2G_{\mathrm{b}}(X-Y)e_{ij}^{O}-\left(\frac{B'}{A'}-1\right)e_{ij}^{\mathrm{K},O}\right] \quad (17)$$

where G_{b} is the shear modulus of bolt.

Only considering the elastic part, the new spherical stress σ^{iso} of B-B model described at the moment of $t+\Delta t$ can be computed as

$$\sigma^{iso}=\frac{1}{3}\sigma_{kk}^{O}+K\Delta\varepsilon_{kk} \quad (18)$$

where σ_{kk}^{O} is the old spherical stress, K is the instantaneous bulk modulus, and $\Delta\ \varepsilon_{kk}$ is the spherical strain increment.

The constitutive model can be compiled in a dynamic link library file by using Visual Studio 2005 or other compiler versions (Li *et al*. 2014). The open-source FLAC^{3D} code is written by using the object-oriented language (C++) and the present user-defined new constitutive model. The program flowchart is shown in Fig. 10.

4.2 Validation of B-B creep model

The creep behavior can be commonly observed in the deep-lying soft rock (Wang *et al*. 2014; Ping *et al*. 2016). To verify the reliability of the present B-B creep constitutive model program, a numerical model of a tunnel with buried depth of 1000 m is established to analyze the creep behavior of the tunnel obtained from the B-B model support, the non-support and the bolt element support (see Fig. 11). The width of the arch tunnel is 6.0 m and the high of the arch tunnel is 4.95 m. The length, width and thickness of the calculation model are adopted as 60 m, 50 m and 50 m, respectively. The length of the bolt is 2.2 m, and the diameter of the bolt is 20 mm. The drilling diameter is taken as 32 mm, and the spacing between two bolts is adopted as 1.0 m. The average density of the rock is adopted as 25 kN/m^3. This suggests that a distributed force of 25 MPa is applied on the top of the calculation model. The basic mechanical parameters of rock in the numerical model can be obtained from the average values in Table 1. The bottom of the calculation model is constrained in the vertical displacement and both sides are constrained in the horizontal displacement, as shown in Fig. 12.

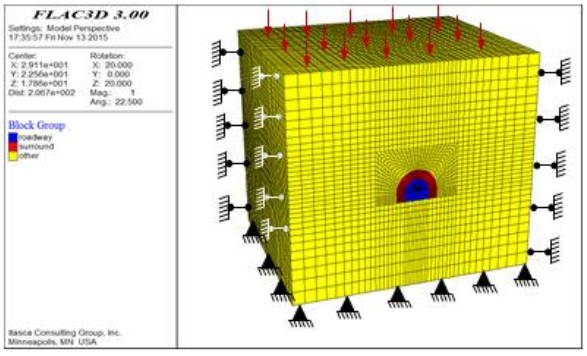

Fig. 12 Three-dimensional model of tunnel

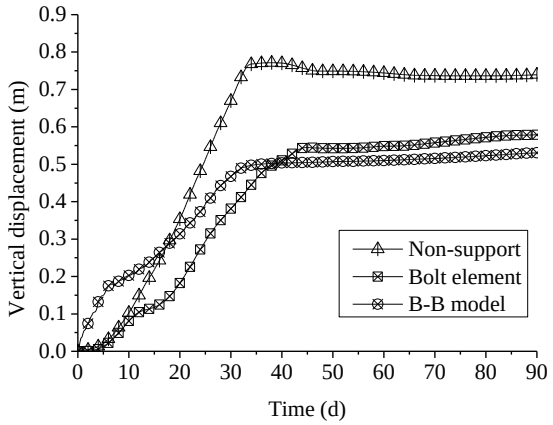

Fig. 13 Relationship between vertical displacement of roof of tunnel and time

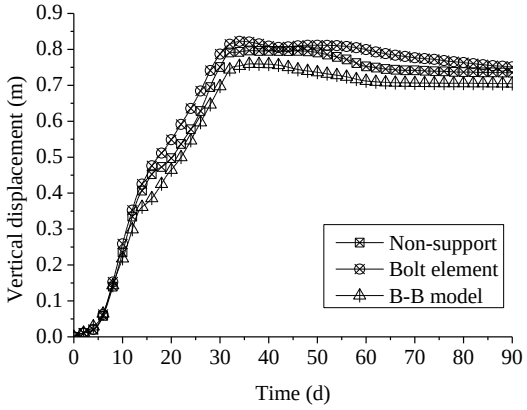

Fig. 14 Relationship between vertical displacement of floor of tunnel and time

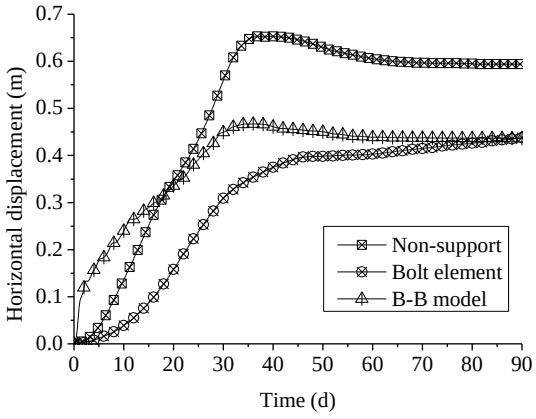

Fig. 15 Relationship between horizontal displacement of middle right roadside of tunnel and time

Table 6 Displacements of different locations of tunnel (time=90 days)

Support model	Arch crown	Spandrel		Midpoint of right wall		Right corner		Midpoint of floor	Convergence time (h)
	u_z (cm)	u_x (cm)	u_z (cm)	u_x (cm)	u_z (cm)	u_x (cm)	u_z (cm)	u_z (cm)	
Non-support	-73.94	-36.13	-62.91	-59.39	-10.16	-20.51	11	73.51	1.24
Bolt element	-57.84	-25.99	-46.2	-43.75	0.09	-19.24	16.97	75.15	1.53
B-B model	-53.06	-27.46	-48.56	-43.62	-14	-19.62	6.532	70.46	0.87

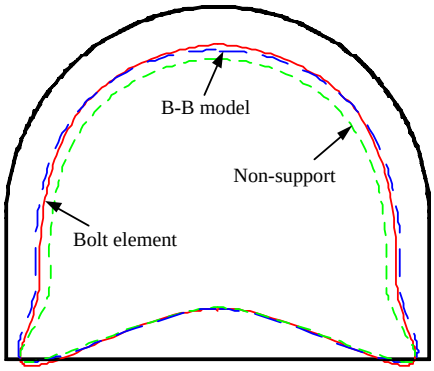

Fig. 16 Deformation convergence of tunnel surface (time=90 days)

The supported range of the bolt element is simulated by using the B-B model. The creep parameters of the B-B model are adopted as follows: E_1 = 126.02 MPa, η_1 = 3019.35 MPa·d, E_2 = 1365.8 MPa, and η_2 = 268.865 MPa·d. Based on the principle of equivalent stiffness, the bolted elastic modulus E_b is calculated as 98.78 MPa (260×103 MPa×3.14×0.022×0.022/4 = 98.78 MPa).

The calculated deformation time of model is 90 days. The relationships between displacement of roof, floor and right surrounding rock of tunnel and time are shown in Figs. 13-15, respectively.

It can be observed from Figs. 13-15 that the creep deformation of surrounding rock derived from three models becomes gradually stable after 30-40 d. Due to the reinforcement of bolts, the creep deformations and the creep rates of roof and roadside of tunnel calculated by using the B-B creep model and the bolt element are smaller. However, the creep tendencies and deformations of floor of tunnel calculated using the above-mentioned three models are the same because the floor of tunnel is not supported.

The displacements of different locations of tunnel (time=90 days) are summarized in Table 6. Fig. 16 shows the convergence deformation of tunnel surface (time=90 days). The calculation results show that the convergence deformation estimated from the present B-B model is consistent with the calculated results of the inherent bolt element in FLAC^{3D}, and the convergence deformation can be more effectively controlled when the proposed B-B model is used in the FLAC^{3D} software. The convergence time of the three support models in Table 6 is 1.24 h, 1.53 h, and 0.87 h, respectively. The computational efficiency of the B-B model is increased by 43.14% compared to that of the bolt element model. This indicated that the present B-B creep model can be used to analyze the creep behavior of surrounding rock of tunnel. The big advantage of the present B-B creep model is that the computational efficiency can be remarkably improved by using the proposed B-B creep model in the FLAC^{3D} software.

5. Conclusions

In this paper, the creep behavior of bolted rock was analyzed by using the unconfined creep tests and the numerical results. Some new foundings are summarized as

below:

• The creep experimental results show that the creep stress level of bolted specimen is 1.2 to 1.3 times that of the non-bolted specimens and the threshold of creep stress is large because of the anchoring effect of bolts. Compared with the bolted specimen, the creep deformation of the non-bolted specimen increases significantly when the load increase from 70% σ_c to 80% σ_c. The strength of red sandstones can be improved, and the failure strength of the bolted specimen is 1.05 to 1.1 times that of the non-bolted specimen.

• Based on the test results, the Bolted Burgers creep model (B-B model) was proposed to clarify the creep mechanism of rock mass due to rock bolts. The deformation of bolts is assumed to be identical to that of rock and the load is shared by bolts and rock. Consequently, the B-B model can be composed of a spring with great stiffness and the Burgers model connected in parallel. The calculated and the experimental creep strains demonstrate that the creep properties of bolted surrounding rock can be well simulated by using the B-B model.

• As to the simulation of the creep behavior of bolted rock, a new user-defined incremental iterative format of the B-B model was established and the open-source FLAC^{3D} code was written by using the object-oriented language (C++). The significance of the development model is that the B-B creep constitutive model can reflect the influence on the creep mechanical behavior of bolted rock due to rock bolts in the numerical simulation.

• To check the reliability of the present B-B creep constitutive model program, a numerical model of a tunnel with buried depth of 1000 m was established to analyze the creep response of the tunnel with the B-B model support, the non-support and the bolt element support. The simulation results show that the present B-B model is consistent with the calculated results of the inherent bolt element in FLAC^{3D}, and the convergence deformation can be more effectively controlled when the proposed B-B model is used in the FLAC^{3D} software. The big advantage of the present B-B creep model secondarily developed in the FLAC^{3D} software is the high computational efficiency.

Acknowledgments

This work was supported by the National Natural Science Foundation of China (No. 51474136, No.51408338, No.51604165), the Shandong Provincial Natural Science Foundation of China (No. ZR2014EEQ009), and the China Postdoctoral Science Foundation Special Funded Project (No. 2014T70641). Great appreciation goes to the editorial board and the reviewers of this paper.

References

Boon, C.W., Houlsby, G.T. and Utili, S. (2015), "Designing tunnel support in jointed rock masses via the DEM", *Rock Mech. Rock Eng.*, **48**(2), 603-632.

Cai, Y., Esaki, T. and Jiang, Y.J. (2004), "A rock bolt and rock mass interaction model", *J. Rock Mech. Min. Sci.*, **41**(7), 1055-1067.

Cai, Y., Jiang, Y.J., Djamaluddin, I., Iura, T. and Esaki, T. (2015), "An analytical model considering interaction behavior of grouted rock bolts for convergence-confinement method in tunneling design", *J. Rock Mech. Min. Sci.*, **76**, 112-126.

Chen, H. (2008), "Model test theoretical analysis of the interaction of the surrounding rock and supporting system of underground engineering", Ph.D. Dissertation, Institute of Rock & Soil Mechanics, Chinese Academy of Sciences, Wuhan, China.

Chen, S.H., Qiang, S., Chen, S.F. and Egger, P. (2004), "Composite element model of the fully grouted rock bolt", *Rock Mech. Rock Eng.*, **37**(3), 193-212.

Deb, D. and Das, K.C. (2014), "A new doubly enriched finite element for modelling grouted bolt crossed by rock joint", *J. Rock Mech. Min. Sci.*, **70**, 47-58.

Kang, H.P., Lin, J. and Fan, M.J. (2015), "Investigation on support pattern of a coal mine roadway within soft rocks-a case study", *J. Coal Geol.*, **140**, 31-40.

Li, Y.J., Zhang, D.L. and Fang, Q. (2014), "A physical and numerical investigation of the failure mechanism of weak rocks surrounding tunnels", *Comput. Geotech.*, **61**, 292-307.

Lopez-Gayarre, F., Fernandez-Rodriguez, R., Gonzalez-Nicieza, C. and Garcia-Menendez, J.R. (2015), "Analysis of viscoelastic behaviour of rock salt using hydraulic cylinder test", *Bull. Eng. Geol. Environ.*, **74**(2), 545-553.

Nemcik, J., Ma, S.Q., Aziz, N., Ren, T. and Geng, X.Y. (2014), "Numerical modelling of failure propagation in fully grouted rock bolts subjected to tensile load", *J. Rock Mech. Min. Sci.*, **71**, 293-300.

Cao, P., Youdao, W., Yixian, W., Haiping, Y. and Bingxiang, Y. (2016), "Study on nonlinear damage creep constitutive model for high-stress soft rock", *Environ. Earth Sci.*, **75**(10), 900.

Selvadurai, A.P.S. (1978), "The time-dependent response of a deep rigid anchor in a viscoelastic medium", *J. Rock Mech. Min. Sci.*, **15**(1), 11-19.

Selvadurai, A.P.S. (1979), "Some results concerning the viscoelastic relaxation of prestress in a surface rock anchor", *J. Rock Mech. Min. Sci.*, **16**(5), 309-317.

Showkati, A., Maarefvand, P. and Hassani, H. (2015), "Theoretical determination of stress around a tensioned grouted anchor in rock", *Geomech. Eng.*, **8**(3), 441-460.

Spang, K. and Egger, P. (1990), "Action of fully-grouted bolts in jointed rock and factors of influence", *Rock Mech. Rock Eng.*, **23**(3), 201-229.

Sun, J. (2007), "Rock rheological mechanics and its advance in engineering applications", *Chin. J. Rock Mech. Eng.*, **26**(6), 1081-1106 (in Chinese).

Tan, Y.L., Liu, X.S., Ning, J.G., Lu, Y.W. (2017), "In situ investigations on failure evolution of overlying strata induced by mining multiple coal seams", *Geotech. Test. J.*, **40**(2), 1-14.

Tan, Y.L., Yu, F.H., Ning, J.G. and Zhao, T.B. (2015), "Design and construction of entry retaining wall along a gob side under hard roof stratum", *J. Rock Mech. Min. Sci.*, **77**, 115-121.

Wang, J.B., Liu, X.R., Liu, X.J. and Huang, M. (2014), "Creep properties and damage model for salt rock under low-frequency cyclic loading", *Geomech. Eng.*, **7**(5), 569-587.

Wang, J.B., Liu, X.R., Song, Z.P. and Shao, Z.S. (2015), "An improved Maxwell creep model for salt rock", *Geomech. Eng.*, **9**(4), 499-511.

Wen, N.D. (2007), "The study of anchorage styles optimization of fractured rock mass on experimental and numerical simulation", M.Sc. Dissertation, Shandong University, Jinan, China.

Wu, W., Jiang, G., Huang, S. and Leo, C.J. (2014), "Vertical dynamic response of pile embedded in layered transversely isotropic soil", *Math. Prob. Eng.*

Yang, M.J., Zhao, Y.M. and Zhang, N. (2014), "Creep behavior of

epoxy-bonded anchor system", *J. Rock Mech. Min. Sci.*, **67**, 96-103.
Zhang, K., Zhang, G.M., Hou, R.B., Wu, Y. and Zhou, H.Q. (2015), "Stress evolution in roadway rock bolts during mining in a fully mechanized longwall face, and an evaluation of rock bolt support design", *Rock Mech. Rock Eng.*, **48**(1), 333-344.
Zhao, T.B., Guo, W.Y., Lu, C.P. and Zhao, G.M. (2016), "Failure characteristics of combined coal-rock with different interfacial angles", *Geomech. Eng.*, **11**(3), 345-359.
Zhao, T.B., Guo, W.Y., Tan, Y.L., Lu, C.P. and Wang, C.W. (2017), "Case histories of rock bursts under complicated geological conditions", *Bull. Eng. Geol. Environ.*, 1-17.

CC